

ON VARIOUS DISPERSION MODELS FOR SIMULATING FLOW AT CHANNEL BENDS^{*}

A. BAGHLANI

Faculty of Civil and Environmental Eng., Shiraz University of Technology, Shiraz, I. R. of Iran
Email: baghlani@sutech.ac.ir

Abstract– In this paper, by using depth-averaged equations, three different dispersion models for simulating flow at channel bends are presented and compared. Two of these models employ power law velocity distributions for longitudinal velocity components and linear distributions for transverse component, and the last model employs logarithmic velocity distributions in transverse and longitudinal directions. The first two models differ in how the effect of secondary flow is evaluated. Boundary-fitted curvilinear coordinates in conjunction with finite-volume method have been used for discretization of the governing equations. The numerical results are compared with available experimental data of a 270° bend. The study shows that a power law distribution for streamwise velocity with a suitable estimation of secondary flow intensity gives the best results for simulation of two-dimensional depth-averaged flow in open channel bends among the models studied. This model can successfully predict the most important characteristics of flow in curved channels.

Keywords– Open channel flow, channel bends, momentum dispersion, secondary flow, depth-averaged flow

1. INTRODUCTION

Many problems in hydraulic engineering can be simulated by depth-averaged models with negligible error. Actually, two-dimensional solutions of the governing equations are more practical in real-life problems, such as simulation of flow in natural rivers and estuaries, since 3D solutions require much more computational effort. Therefore, in dealing with practical problems, 2D and even 1D solution are preferred. Depth-averaging greatly simplifies the problem, but 3D features of flow in some problems are ignored. In many cases, such as flow in straight channels, this ignored information is negligible and satisfactory results can be obtained. If they are available for engineers, two-dimensional simulations of flow can also be accomplished by some commercial software [1]. Unfortunately, natural rivers are seldom straight and simulation of flow in river bends by simplified models needs more consideration. Indeed, centrifugal forces at river bends form secondary or helical flows in which the fluid particles on the free surface tend to transfer from the inner bank to the outer bank and particles near the bed shift from the outer bank to the inner bank. This phenomenon is automatically included in 3D models because of vertical grids, but can produce significant errors in 2D models if it is neglected.

To consider the effect of 3D features of flow in 2D models caused by helical flows, dispersion terms are added in the momentum equations. In other words, the shear stresses caused by secondary flow are included in the model.

Several models are available to evaluate dispersion terms in channel bends. Rozovskii [2] was one of the pioneers who studied flow in channel bends and derived a fairly complicated formulation for

^{*}Received by the editors February 8, 2012; Accepted November 5, 2012.

secondary flow phenomena. Kikkawa et al. [3] suggested an equation for secondary flow based on the stream function. Flokestra emphasized that dispersion terms are required for correct simulation of flow in channel bends [4]. De Vriend derived a governing equation for estimation of secondary flow intensity [5]. Odgaard [6] made a simplification to Rozovskii's model and proposed a linear distribution for the transverse velocity which is extensively used by other researchers [7, 8]. Baek et al. developed expressions for transverse and streamwise velocity profiles, which are based on Odgaard's model [9]. Zeng et al. studied flow in sharp bends numerically and experimentally [10]. Seo and Jung reviewed the theoretical equations of transverse velocity profiles and concluded that Kikkawa et al. and Baek et al.'s formulations are able to represent the characteristics of streamwise and transverse velocities within channel bends [11]. Begnudelli et al. [7] formulated a two-dimensional numerical model for describing flow hydrodynamic, sediment transport and bed evolution in curved channels. Ottewanger et al. formulated a model for flow redistribution and helical flows and compared the results from their model with three sets of experiments and concluded that the model does represent the velocity redistribution in bends and meanders [12]. Motta et al. also derived a simplified two-dimensional model to simulate the flow, sediment transport and migration of bends and meanders [13].

In the current study, three different approaches for modeling dispersion terms are presented and compared. In the first model, a power law velocity distribution is assumed to be valid in streamwise direction and the transverse velocity at the water surface is estimated. The second model is similar to the first, but secondary flow intensity is estimated by an analytical approach. The third model uses logarithmic velocity distributions in longitudinal and transverse directions. Turbulence shear stresses are also included in this model to enhance the accuracy of the scheme. Finite-volume discretization of the equations is adopted and a standard Godunov scheme is used for evaluation of numerical flux at cell interfaces. Instead of using an unstructured grid (e.g. [7, 14]) or adopting a very common coordinate system along the longitudinal and transverse directions (e.g. [6, 11, 15]), the method of boundary-fitted curvilinear coordinates which is very flexible and robust, has been employed. Experimental bend data from Steffler [16] have been used to investigate the capability of each model in simulating the main characteristics of flow in channel bends.

2. SHALLOW WATER EQUATIONS

Two-dimensional equations of flow can be written as follows:

$$\frac{\partial U}{\partial t} + \frac{\partial F}{\partial x} + \frac{\partial G}{\partial y} = \frac{\partial M}{\partial x} + \frac{\partial N}{\partial y} + S \quad (1)$$

$$U = \begin{bmatrix} h \\ hu \\ hv \end{bmatrix}, F = \begin{bmatrix} hu \\ hu^2 + gh^2/2 \\ huv \end{bmatrix}, G = \begin{bmatrix} hv \\ huv \\ hv^2 + gh^2/2 \end{bmatrix}$$

$$M = \begin{bmatrix} 0 \\ \vartheta^t h \frac{\partial u}{\partial x} + \frac{\partial(hD_{xx})}{\partial x} \\ \vartheta^t h \frac{\partial v}{\partial x} + \frac{\partial(hD_{yx})}{\partial x} \end{bmatrix}, N = \begin{bmatrix} 0 \\ \vartheta^t h \frac{\partial u}{\partial y} + \frac{\partial(hD_{xy})}{\partial x} \\ \vartheta^t h \frac{\partial v}{\partial y} + \frac{\partial(hD_{yy})}{\partial x} \end{bmatrix}, S = \begin{bmatrix} 0 \\ -\frac{\tau_{bx}}{\rho} - ghS_{0x} \\ -\frac{\tau_{by}}{\rho} - ghS_{0y} \end{bmatrix} \quad (2)$$

in which h is water depth; u, v are depth-averaged velocities in x and y directions, respectively; τ_{bx}, τ_{by} are bed shear stresses in x and y directions, respectively; S_{0x}, S_{0y} are bed slopes in two directions; g is gravitational acceleration; ρ is the water density; and ϑ^t is kinematic eddy viscosity related to turbulence. Moreover, D_{xx}, D_{xy}, D_{yx} and D_{yy} are dispersion terms due to the presence of secondary flows in channel bends. These terms are negligible in nearly straight channels, but have crucial importance in simulating flow in channel bends.

Bed shear stresses are related to the depth-averaged flow velocities as:

$$\tau_{bx} = c_f \rho u \sqrt{u^2 + v^2}, \quad \tau_{by} = c_f \rho v \sqrt{u^2 + v^2} \quad (3)$$

in which c_f is bed friction that can be related to Chezy coefficient, C (i.e. $c_f = \frac{g}{C^2}$). Kinematic eddy-viscosity can be computed as follows:

$$\vartheta^t = \frac{\kappa}{6} u_* h \quad (4)$$

in which κ is von Karman coefficient $\kappa = 0.4$, and u_* is the shear velocity:

$$u_* = \sqrt{c_f (u^2 + v^2)} \quad (5)$$

3. TRANSFORMED BOUNDARY-FITTED EQUATIONS

Generally, unstructured grids and channel-fitted coordinate systems, in which the governing equations are written in terms of streamwise and transverse directions, are the most common approaches to deal with flows in channel bends. However, the powerful boundary-fitted curvilinear coordinate system is adopted in this study. In boundary-fitted curvilinear coordinates, the complex physical domain is mapped to a rectangular domain. Although the procedure introduces extra non-linearity into the governing equations, the imposition of boundary conditions is straightforward and computer coding is extensively simplified. Eq. (6) relates derivatives of a variable in the physical domain, (x, y) , to the computational domain, (ξ, η) [17]:

$$\begin{pmatrix} \frac{\partial}{\partial x} \\ \frac{\partial}{\partial y} \end{pmatrix} = \frac{1}{J} \begin{bmatrix} y_\eta & -y_\xi \\ -x_\eta & x_\xi \end{bmatrix} \begin{pmatrix} \frac{\partial}{\partial \xi} \\ \frac{\partial}{\partial \eta} \end{pmatrix} \quad (6)$$

the system of equations (1) can be transformed to the following equation:

$$\frac{\partial \tilde{U}}{\partial t} + \frac{\partial \tilde{F}}{\partial x} + \frac{\partial \tilde{G}}{\partial y} = \tilde{P} \quad (7)$$

In the aforementioned equations $x_\xi, x_\eta, y_\xi, y_\eta$ are called the metrics of transformation in which subscripts imply the derivative with respect to coordinates in computational domain, $J = x_\xi y_\eta - x_\eta y_\xi$ is the determinant of the Jacobian of the transformation. Moreover, the following equations for the variables in Eq. (7) can be obtained after applying Eq. (6) to (1):

$$\tilde{U} = JU, \quad \tilde{F} = y_\eta F - x_\eta G, \quad \tilde{G} = -y_\xi F + x_\xi G, \quad \tilde{P} = JP \quad (8)$$

$$P = \begin{pmatrix} 0 \\ P_{21} \\ P_{31} \end{pmatrix}$$

$$P_{21} = \frac{1}{J} \frac{\partial}{\partial \xi} \left\{ \frac{\vartheta^t h}{J} \left[(y_\eta^2 + x_\eta^2) \frac{\partial u}{\partial \xi} - (y_\xi y_\eta + x_\xi x_\eta) \frac{\partial u}{\partial \eta} \right] \right\} + \frac{1}{J} \frac{\partial}{\partial \eta} \left\{ \frac{v^t h}{J} \left[-(y_\xi y_\eta + x_\xi x_\eta) \frac{\partial u}{\partial \xi} + (y_\xi^2 + x_\xi^2) \frac{\partial u}{\partial \eta} \right] \right\} + \frac{1}{J} \left[\frac{\partial(hD_{xx})}{\partial \xi} y_\eta - \frac{\partial(hD_{xx})}{\partial \eta} y_\xi \right] + \frac{1}{J} \left[-\frac{\partial(hD_{xy})}{\partial \xi} x_\eta + \frac{\partial(hD_{xy})}{\partial \eta} x_\xi \right] - \frac{\tau_{bx}}{\rho} - ghS_{0x}$$

$$P_{31} = \frac{1}{J} \frac{\partial}{\partial \xi} \left\{ \frac{\vartheta^t h}{J} \left[(y_\eta^2 + x_\eta^2) \frac{\partial v}{\partial \xi} - (y_\xi y_\eta + x_\xi x_\eta) \frac{\partial v}{\partial \eta} \right] \right\} + \frac{1}{J} \frac{\partial}{\partial \eta} \left\{ \frac{v^t h}{J} \left[-(y_\xi y_\eta + x_\xi x_\eta) \frac{\partial v}{\partial \xi} + (y_\xi^2 + x_\xi^2) \frac{\partial v}{\partial \eta} \right] \right\} + \frac{1}{J} \left[\frac{\partial(hD_{yx})}{\partial \xi} y_\eta - \frac{\partial(hD_{yx})}{\partial \eta} y_\xi \right] + \frac{1}{J} \left[-\frac{\partial(hD_{yy})}{\partial \xi} x_\eta + \frac{\partial(hD_{yy})}{\partial \eta} x_\xi \right] - \frac{\tau_{by}}{\rho} - ghS_{0y} \quad (9)$$

The unit vectors tangential to the ξ and η directions are [18, 19]:

$$\vec{e}_\xi = \frac{1}{g_{11}} (x_\xi \vec{i} + y_\xi \vec{j}) \quad : \text{ tangential to } \xi \quad (10.1)$$

$$\vec{e}_\eta = \frac{1}{g_{22}}(x_\eta \vec{i} + y_\eta \vec{j}) \quad : \text{ tangential to } \eta \quad (10.2)$$

in which

$$g_{11} = \sqrt{x_\xi^2 + y_\xi^2} \quad , \quad g_{22} = \sqrt{x_\eta^2 + y_\eta^2} \quad (11)$$

Therefore, the components of velocity in the streamwise and transverse directions in curvilinear coordinates can be readily found by the dot product of the velocity vector and the corresponding unit vectors as follows:

$$u_\xi = u_s = \frac{1}{g_{11}}(u x_\xi + v y_\xi) \quad : \text{ component of velocity in streamwise direction} \quad (12.1)$$

$$u_\eta = u_t = \frac{1}{g_{22}}(u x_\eta + v y_\eta) \quad : \text{ component of velocity in streamwise direction} \quad (12.2)$$

4. DISPERSION MODELING

Spiral movement of the fluid particles in the channel bends develops secondary currents that cause redistribution of streamwise velocity toward the outer bank. In 3D models, the secondary currents are included in the model because of the vertical grid. However, depth-averaging the 3D equations causes loss of important information of the flow in the vertical direction. In straight channels the loss of accuracy has been found to be negligible. Yet, for channel bends, important features of 3D flow should be considered in 2D models to improve the accuracy of the simulation. Therefore, shear stresses due to presence of secondary flow are included in the 2D depth-averaged models by dispersion terms D_{xx} , D_{xy} , D_{yx} and D_{yy} in the governing Eqs. (1) and (2). Dispersion terms appear after integrating the 3D governing equations in the vertical direction and can be evaluated as follows [20]:

$$\begin{aligned} D_{xx} &= -\frac{1}{h} \int_0^h (u(z) - u)^2 dz \\ D_{xy} = D_{yx} &= -\frac{1}{h} \int_0^h (u(z) - u)(v(z) - v) dz \\ D_{yy} &= -\frac{1}{h} \int_0^h (v(z) - v)^2 dz \end{aligned} \quad (13. 1,2,3)$$

in which $u(z)$ and $v(z)$ are the velocity distributions in x and y directions, respectively and z denotes the vertical direction. In order to evaluate the dispersion terms, velocity distributions are required in the streamwise and transverse directions. Similar equations, to Eq. (13) can be written for the dispersion terms in the streamwise and transverse directions, provided that the velocity distributions are considered in those directions. Depending on the velocity profile chosen, various dispersion models can be used. In this study, three different approaches for dispersion modeling are presented and compared. In the first two models, a linear distribution for the transverse component of velocity proposed by Odgaard [6] has been adopted and the models differ from each in how the effects of helical motion are modeled. The third model employs a logarithmic velocity distribution.

It is worthy to recall that the Odgaard's distribution for transverse velocity has been widely adopted in the literature as mentioned in the introduction. The transverse velocity distribution can be written as follows [6]:

$$u_t(z) = u_t + v_s \left(2 \frac{z}{h} - 1\right) \quad (14)$$

in which $u_t(z)$ is local transverse velocity at height z , u_t is depth-averaged transverse velocity which can be calculated from Eq. 12(b) in the curvilinear coordinate system, and v_s is the transverse velocity at the free surface.

In the following subsections the various models for estimating the dispersion terms are presented.

MODEL 1: power law velocity distribution, estimation of v_s

Power law distribution for streamwise component of velocity reads [20]:

$$u_s(z) = \frac{m+1}{m} u_s \left(\frac{z}{h}\right)^{\frac{1}{m}} \tag{15}$$

in which $u_s(z)$ is local streamwise velocity at height z , u_s is depth-averaged streamwise velocity which can be calculated using Eq. (12.1) in the curvilinear coordinate system. Moreover, m is a function of bed roughness and defined as:

$$m = \kappa C / \sqrt{g} \tag{16}$$

in which $\kappa = 0.4$ is Von Karman's constant.

Integrating Eqs. (13) using velocity profiles (14) and (15) gives the following equations for the dispersion terms in streamwise and transverse directions:

$$D_{ss} = -\frac{u_s^2}{m(2+m)}, \quad D_{st} = -\frac{u_s v_s}{1+2m}, \quad D_{tt} = -\frac{v_s^2}{3} \tag{17}$$

Subscripts s and t have been used as a reminder that these expressions have been evaluated in streamwise and transverse directions, respectively.

In this model, the transverse surface velocity is estimated as follows [7]:

$$v_s = \frac{2m+1}{2\kappa^2 m} \frac{h}{r} u_s \tag{18}$$

in which r is the local radius of curvature.

In boundary-fitted curvilinear coordinates, the following relations were derived for transformation of dispersion terms from streamwise and transverse directions to those of x and y directions:

$$\begin{aligned} D_{xx} &= \alpha_{11}\alpha_{11}D_{ss} + 2\alpha_{11}\alpha_{12}D_{st} + \alpha_{12}\alpha_{12}D_{tt} \\ D_{xy} &= \alpha_{11}\alpha_{21}D_{ss} + 2(\alpha_{11}\alpha_{22} + \alpha_{12}\alpha_{21})D_{st} + \alpha_{12}\alpha_{22}D_{tt} \\ D_{yy} &= \alpha_{21}\alpha_{21}D_{ss} + 2\alpha_{21}\alpha_{22}D_{st} + \alpha_{22}\alpha_{22}D_{tt} \end{aligned} \tag{19}$$

where

$$\alpha_{11} = \frac{1}{j} g_{22} x_\xi, \quad \alpha_{12} = \frac{1}{j} g_{11} x_\eta, \quad \alpha_{21} = \frac{1}{j} g_{22} y_\xi, \quad \alpha_{22} = \frac{1}{j} g_{11} y_\eta \tag{20}$$

MODEL 2: Power law velocity distribution, evaluating the secondary flow intensity

In Odgaard's model, the transverse velocity at the free surface can be related to secondary flow intensity I as follows [20]:

$$v_s = I b_s \tag{21}$$

Theoretically, the secondary flow intensity I is $I = \frac{h}{r} u_s$ [5]. Having this in mind and comparing Eqs. (18) and (21) reveals that:

$$b_s = \frac{2m+1}{2\kappa^2 m} \tag{22}$$

In this model, the secondary flow intensity is estimated directly and replaced in Eq. (21). The rest of the procedure is similar to Model 1.

According to De Vriend [5], the following equation holds for the secondary flow intensity [5, 20]:

$$\frac{\partial(hI)}{\partial t} + \frac{\partial(huI)}{\partial x} + \frac{\partial(hvI)}{\partial y} = \frac{\partial}{\partial x} \left(D_I h \frac{\partial I}{\partial x} \right) + \frac{\partial}{\partial y} \left(D_I h \frac{\partial I}{\partial y} \right) - \frac{h}{T_a} \left(I - \frac{\beta_I h u_s}{r} \right) \quad (23)$$

in which D_I is the diffusion and dispersion coefficient of I , T_a is the adaptation time of I and β_I is in the range of 1.0-2.0.

To estimate I , Eq. (23) should be solved numerically and therefore, the computational effort increases. Wu and Wang proposed the following analytical solution of Eq. (23) after some simplifications [21]:

$$\frac{rI}{\beta_I h u_s} = 1 - \frac{1-e^{-\psi}}{e^{\psi}-e^{-\psi}} e^{\psi y'} - \frac{1-e^{\psi}}{e^{\psi}-e^{-\psi}} e^{-\psi y'} \quad (24)$$

where

$$\psi = \frac{W}{\sqrt{T_a D_I}} \quad (25)$$

and the term $T_a D_I$ can be estimated as follows:

$$T_a D_I = \frac{\lambda_t r_c h \sqrt{g}}{c} \quad (26)$$

In the above equations, r_c is the radius of curvature at the channel centerline, W is the channel width and λ_t has a value about 3.0 [20]. In addition, $y' = y/W$ is the dimensionless transverse coordinate with $y' = 0$ at the inner bank and $y' = 1$ at the outer bank.

Model 3: Logarithmic velocity distributions

In this model, the logarithmic velocity distributions in streamwise and transverse directions proposed by De Vriend [22] and Rozovskii [2] are adopted:

$$u_s(z) = u_s \left(1 + \frac{1}{m} + \frac{\ln \zeta}{m} \right) \quad (27)$$

$$u_t(z) = u_t \left(1 + \frac{1}{m} + \frac{\ln \zeta}{m} \right) + \frac{u_s h}{\kappa^2 r} \left[F_1(\zeta) - \frac{1}{m} [F_2(\zeta) + 0.8(1 + \ln \zeta)] \right] \quad (28)$$

in which $\zeta = z/h$ is dimensionless distance from the bed, m has already been defined in Eq. (16) and also:

$$F_1(\zeta) = \int_0^1 \frac{2 \ln \zeta}{\zeta-1} d\zeta = \frac{\pi^2}{3} \quad (29)$$

$$F_2(\zeta) = \int_0^1 \frac{(\ln \zeta)^2}{\zeta-1} d\zeta \approx -2.404 \quad (30)$$

Substituting in Eq. (13) and integrating gives the following equations for the dispersion terms in the streamwise and transverse directions [22, 23]:

$$D_{ss} = -\frac{u_s^2 h}{m^2} \quad (31)$$

$$D_{st} = -\left[\frac{h u_t^2}{m^2} + \frac{u_s^2 h^3}{\kappa^4 r^2} F F_2 + \frac{2 u_s v_s h^2}{m \kappa^2 r} F F_1 \right] \quad (32)$$

$$D_{st} = -\left[\frac{h u_s v_s}{m^2} + \frac{u_s^2 h^2}{m \kappa^2 r} F F_1 \right] \quad (33)$$

where

$$F F_1 = \int_0^1 (1 + \ln \zeta) \left[F_1(\zeta) - \frac{F_3(\zeta)}{m} \right] d\zeta \quad (34)$$

$$F F_2 = \int_0^1 \left[F_1(\zeta) - \frac{F_3(\zeta)}{m} \right]^2 d\zeta \quad (35)$$

$$F_3(\zeta) = [F_2(\zeta) + 0.8(1 + \ln \zeta)] \quad (36)$$

The aforementioned integrals can be calculated numerically. Next, dispersion terms can be computed in x and y directions by means of Eq. (19).

5. EFFECT OF SECONDARY FLOW ON DIRECTION OF BED SHEAR STRESS

In straight channels, direction of bed shear stress is along the direction of mean flow. However, development of secondary flow in bends deviates the direction of bed shear stress relative to mean flow by an angle δ which can be determined by [24]:

$$\delta = \arctan\left(\frac{v}{u}\right) - \arctan\left(A\frac{h}{r}\right) \tag{37}$$

in which A can be defined as [24]:

$$A = \frac{2}{\kappa^2} \left(1 - \frac{1}{m}\right) \tag{38}$$

6. NUMERICAL SOLUTION OF GOVERNING EQUATIONS

Several numerical methods can be used to solve the system of Eqs. (7). In this study, a Godunov scheme in conjunction with the finite volume method is adopted. Since this numerical scheme is well-known, a brief review of the procedure is presented here and the interested reader is referred to relevant references for more details [25-27].

Integrating (7) over a control volume ($d\xi d\eta$), applying divergence theorem, and approximating the line integral, the following equation yields [27]:

$$\frac{\partial \bar{U}_{i,j}}{\partial t} = \tilde{F}_{i,j} - \tilde{F}_{i+1,j} + \tilde{G}_{i,j} - \tilde{G}_{i,j+1} + \tilde{P} \tag{39}$$

It is worthy to note that since the spatial increments $\Delta\xi$ and $\Delta\eta$ can be chosen arbitrarily over the computational domain, they have been set to unity for simplicity.

Godunov solution of (39) relies on evaluating the fluxes \tilde{F} and \tilde{G} by means of an approximate Riemann solver. Here, a Roe's approximate Riemann solver has been used [26-28]:

$$\tilde{F}_{i,j} = \frac{1}{2} \{ \tilde{F}(U_{i,j}^+) + \tilde{F}(U_{i,j}^-) - |A_\xi| (U_{i,j}^+ - U_{i,j}^-) \} \tag{40.1}$$

$$\tilde{G}_{i,j} = \frac{1}{2} \{ \tilde{G}(U_{i,j}^+) + \tilde{G}(U_{i,j}^-) - |A_\eta| (U_{i,j}^+ - U_{i,j}^-) \} \tag{40.2}$$

in which $U_{i,j}^+$ and $U_{i,j}^-$ are the reconstructed states at the right and left sides of the cell interfaces between cells i and j , respectively; A_ξ and A_η are the flux Jacobians in ξ and η directions, respectively. These matrices can be computed as follows:

$$|A_\xi| = R_\xi |\Lambda_\xi| L_\xi \quad , \quad |A_\eta| = R_\eta |\Lambda_\eta| L_\eta \tag{41}$$

where R_ξ and R_η are the right eigenvectors of A_ξ and A_η :

$$R_\xi = \begin{bmatrix} 0 & g_{22} & g_{22} \\ x_\eta & ug_{22} - cy_\eta & ug_{22} + cy_\eta \\ y_\eta & cx_\eta + vg_{22} & -cx_\eta + vg_{22} \end{bmatrix}, \quad R_\eta = \begin{bmatrix} 0 & g_{11} & g_{11} \\ x_\xi & ug_{11} + cy_\xi & ug_{11} - cy_\xi \\ y_\xi & -cx_\xi + vg_{11} & cx_\xi + vg_{11} \end{bmatrix} \tag{42}$$

L_ξ and L_η are the left eigenvectors of A_ξ and A_η :

$$L_\xi = \begin{bmatrix} \frac{ux_\eta + vy_\eta}{g_{22}^2} & \frac{-x_\eta}{g_{22}^2} & \frac{-y_\eta}{g_{22}^2} \\ \frac{uy_\eta - vx_\eta}{2cg_{22}} + \frac{1}{2} & \frac{-y_\eta}{2cg_{22}} & \frac{x_\eta}{2cg_{22}} \\ \frac{-uy_\eta + vx_\eta}{2cg_{22}} + \frac{1}{2} & \frac{y_\eta}{2cg_{22}} & \frac{-x_\eta}{2cg_{22}} \end{bmatrix}, \quad L_\eta = \begin{bmatrix} \frac{-ux_\xi - vy_\xi}{g_{11}^2} & \frac{x_\xi}{g_{11}^2} & \frac{y_\xi}{g_{11}^2} \\ \frac{-uy_\xi + vx_\xi}{2cg_{11}} + \frac{1}{2} & \frac{y_\xi}{2cg_{11}} & \frac{-x_\xi}{2cg_{11}} \\ \frac{uy_\xi - vx_\xi}{2cg_{11}} + \frac{1}{2} & \frac{-y_\xi}{2cg_{11}} & \frac{x_\xi}{2cg_{11}} \end{bmatrix} \quad (43)$$

$|\Lambda_\xi|$ and $|\Lambda_\eta|$ are diagonal matrices entailing the absolute eigenvalues of A_ξ and A_η :

$$|\Lambda_\xi| = \begin{bmatrix} |uy_\eta - vx_\eta| & 0 & 0 \\ 0 & |uy_\eta - vx_\eta - cg_{22}| & 0 \\ 0 & 0 & |uy_\eta - vx_\eta + cg_{22}| \end{bmatrix} \quad (44a)$$

$$|\Lambda_\eta| = \begin{bmatrix} |-uy_\xi + vx_\xi| & 0 & 0 \\ 0 & |-uy_\xi + vx_\xi - cg_{11}| & 0 \\ 0 & 0 & |-uy_\xi + vx_\xi + cg_{11}| \end{bmatrix} \quad (44b)$$

In the aforementioned equations c is wave celerity defined as:

$$c = \sqrt{gh} \quad (45)$$

For reconstruction of states at the left and right faces of the cell interfaces a standard "minmod" limiter has been employed. Equation (39) is integrated numerically over time using a second-order Runge-Kutta method.

7. SIMULATION RESULTS

To compare the effectiveness of the three dispersion models discussed in section 4 in simulation of flow at channel bends, the Steffler's experiment has been selected [16]. The main reasons for selecting this experiment were two. Firstly, a reliable set of data is available in this test for comparison. Secondly, many researchers have used the experimental data of this test to verify their numerical methods (e.g. [8, 14]).

Steffler's bend consists of a straight entrance channel 6.13 m in length followed by a 270° bend with centerline radius of curvature equal to 3.125 m, and a 2.53 m-long straight exit channel (Fig. 1). The flume width was $2b=W=1.07$ m with a Chezy roughness coefficient equal to $50 \text{ m}^{\frac{1}{2}}/\text{s}$. The channel slope was 0.0083. The flow discharge was 23.5 l/s which has been imposed as the inflow boundary condition in the numerical model and the downstream water depth was 6.1 cm which has been imposed as the outflow boundary condition. The zero cross-flow boundary condition is imposed at solid walls.

The experimental flume has been simulated by the model with 259×20 cells in streamwise and transverse directions, respectively. A finer mesh has no significant influence on the results. The computational mesh is shown in Fig. 2.

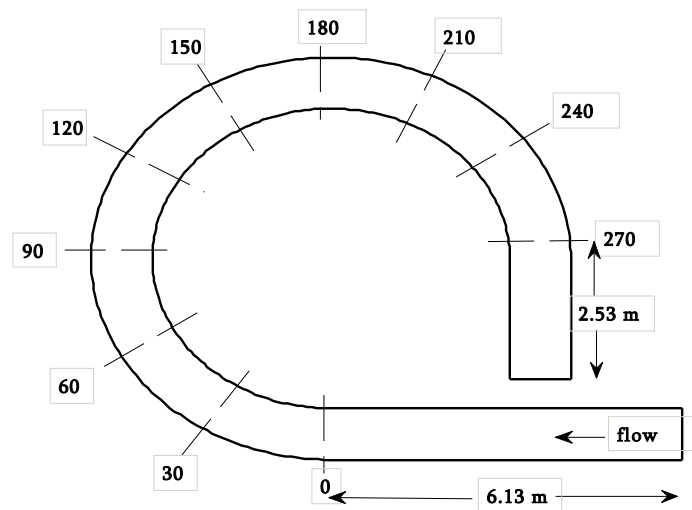


Fig. 1. Schematic plan of Steffler's (1984) experiment

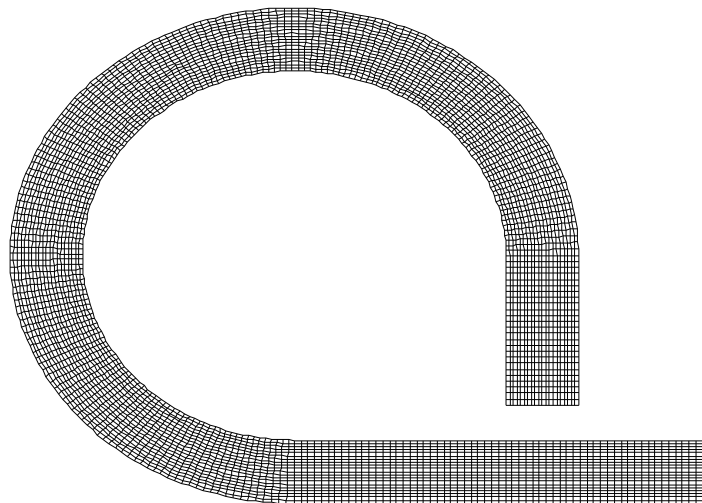


Fig. 2. Computational grid used for analysis of Steffler's (1984) bend

Figure 3 compares the experimental data for water depths at four different cross sections, e.g. at 0° , 90° , 180° and 270° , with simulation results including and discarding the dispersion terms in governing equations. In these figures, $y/b=-1$ indicates the left (outer) bank and $y/b=1$ indicates the right (inner) bank in which b is half channel width. As the figures show, considering dispersion terms in momentum equations has no significant influence in estimating water depth in the channel bend. A satisfactory agreement with experimental data of water depth is obtained even if the dispersion terms are neglected. The results for all three dispersion models in estimating water surface profile were nearly identical, so only one of them has been depicted in these figures. Table 1 reports root-mean-square error (RMSE) of estimating water depth at each cross section when dispersion terms are included or neglected in the model. Root mean square error can be calculated as:

$$RMSE = \sqrt{\frac{\sum_{i=1}^n (P_i - O_i)^2}{n}} \tag{46}$$

in which P is predicted values, O is observed values and n is the number of data.

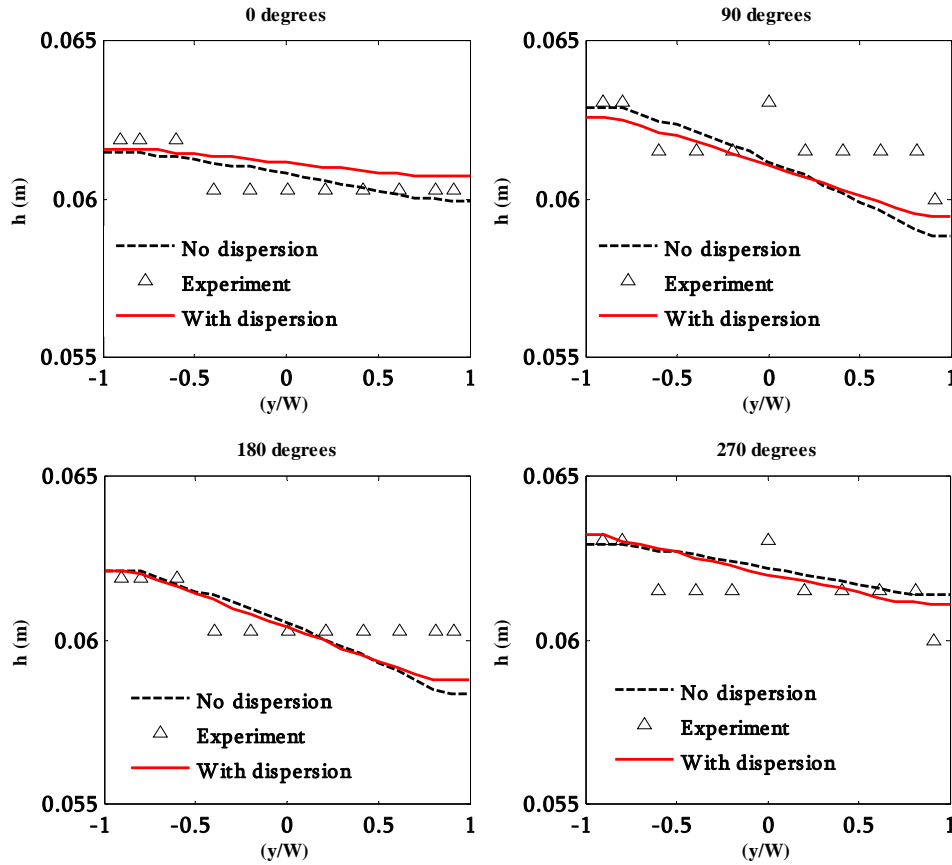


Fig. 3. Comparison of water depth with experimental data of Steffler's bend at four different cross sections

Table 1. Root-mean-square error (RMSE) of water depth (m)

Model	Cross Section (degrees)				Average RMSE
	0	90	180	270	
No Dispersion	0.0055	0.0048	0.0039	0.0012	0.0039
With Dispersion	0.0050	0.0026	0.0012	0.0009	0.0024

Figure 4 shows the contour plot of water depth in the flume; similar results have been obtained for water depth neglecting or taking the dispersion terms into account. However, remarkable differences exist in the results of streamwise velocities if the effect of secondary flow is ignored. Figure 5 compares the results obtained in estimating longitudinal (streamwise) velocity, u_s , for each of three dispersion models with the experimental data. Table 2 reports root-mean-square error (RMSE) of estimating water depth at each cross section when dispersion terms are included using each model or neglected. As Table 2 shows, in all cross sections Model 2 shows the best agreement with experiments and has the least error. In all models, the largest error exists at the inner bank of cross sections 240° and 270° . However, the predictions are satisfactory away from the walls. The results show when the effect of secondary flow is ignored, the streamwise velocity component tends to be nearly uniform across the width of channel; model 1 shows a similar trend. Model 3, in which logarithmic velocity distribution was assumed to be valid, has fairly satisfactory results as well. As cross section 0° in Fig. 5 shows, the predicted streamwise velocity distribution across the width of channel is nearly uniform before entering the bend. Then the maximum

velocity occurs at the inner bank at cross sections 30° and 60° . Next, again the velocity becomes approximately uniform at cross section 90° , 120° and 150° . Finally, the location of maximum velocity shifts to outer bank at the remaining cross sections. Since such typical trends were already observed by other researchers such as Rozovskii [2], Yen [29] and Ghamry and Steffler [14], this means that Models 2 and 3 have been able to predict the phenomenon successfully. Better results can probably be obtained by the model 1, if the radius of curvature of streamlines is estimated and included in the model by a proper approach [7].

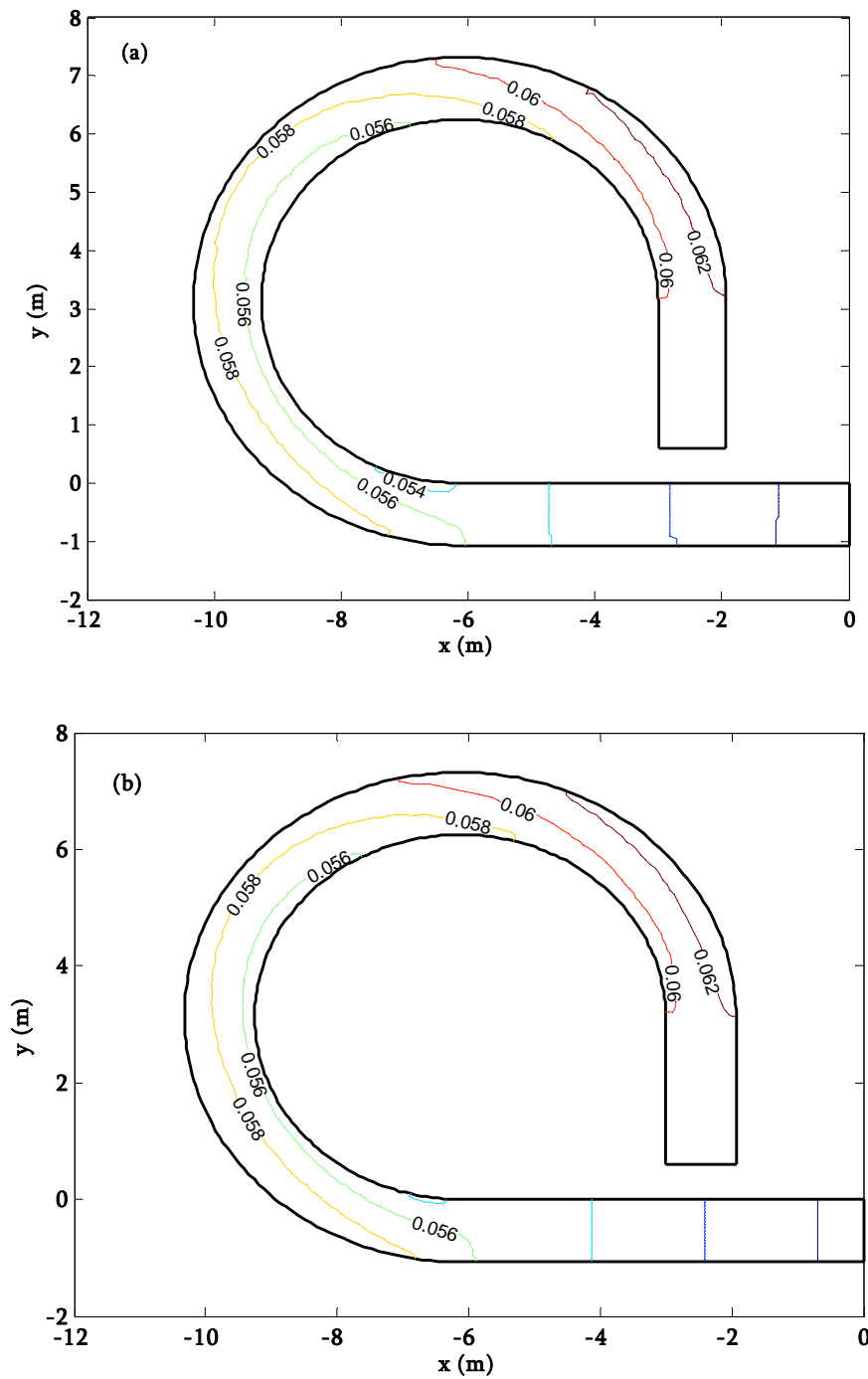


Fig. 4. Contour plot of water depth for Steffler's bend
 (a) without dispersion (b) with dispersion

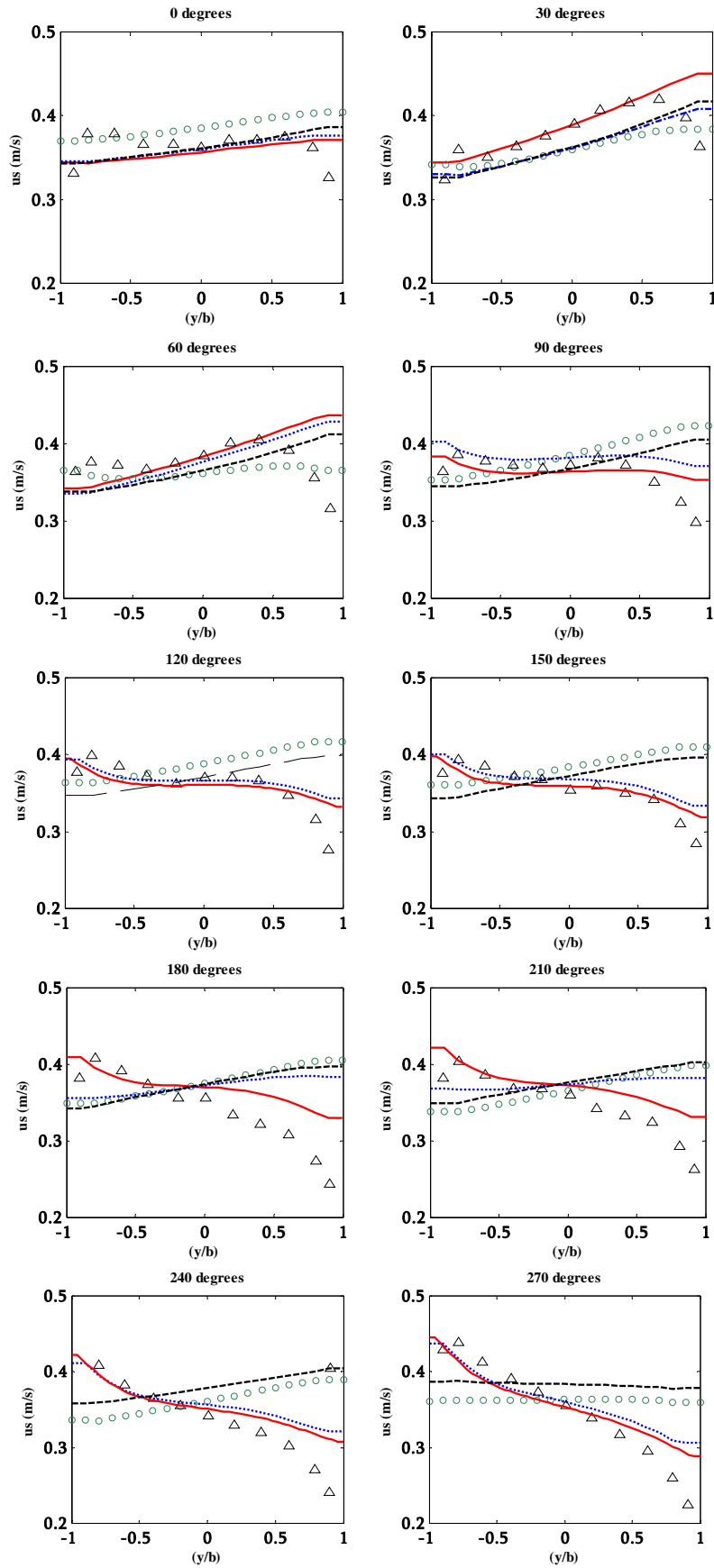


Fig. 5. Comparison of streamwise velocities with experimental data of Steffler's bend at ten different cross sections (Triangles: Experiment, Green circles: No dispersion, Dashed black: Model 1, Solid red: Model 2, Dotted blue: Model 3)

Table 2. Root-mean-square error (RMSE) of streamwise velocities for various models (m/s)

Model	Cross Section (degrees)										Average RMSE
	0	30	60	90	120	150	180	210	240	270	
No Disp.	0.0462	0.0308	0.0462	0.0541	0.0590	0.0566	0.0765	0.0642	0.0737	0.0674	0.0575
Model 1	0.0247	0.0283	0.0396	0.0454	0.0516	0.0511	0.0739	0.0644	0.0781	0.0725	0.0530
Model 2	0.0219	0.0273	0.0258	0.0228	0.0246	0.0203	0.0397	0.0319	0.0483	0.0439	0.0307
Model 3	0.0222	0.0276	0.0378	0.0449	0.0501	0.0478	0.0661	0.0535	0.0632	0.0642	0.0477

Figure 6 illustrates the effect of helical flow in redistribution of velocity in the bend. In part (a) of this figure the secondary flow effects were discarded whereas in part (b) these effects were included in the simulation via Model 2. As the figures show, dispersion terms due to secondary flow have a crucial influence on the velocity field and should be included in 2D models to enhance the accuracy of the numerical schemes.

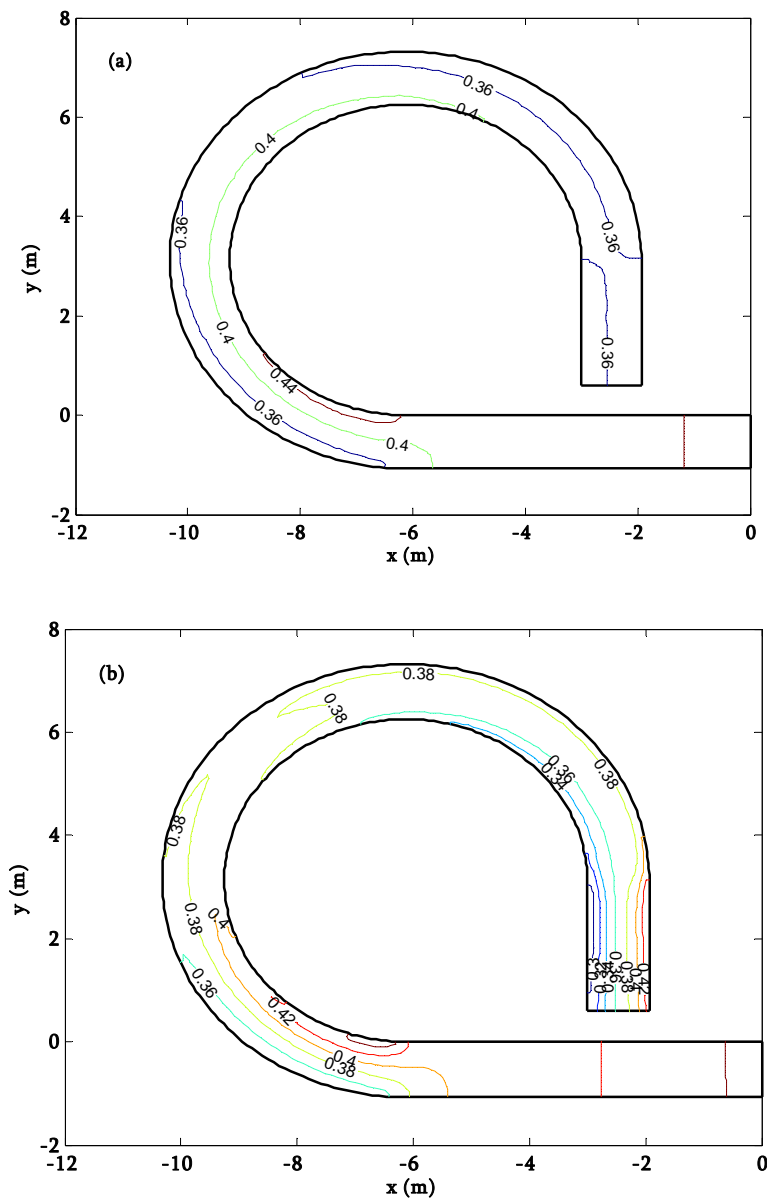


Fig. 6. Contour plot of streamwise velocity for Steffler's bend (a) without dispersion (b) with dispersion

7. SUMMARY AND CONCLUSION

Three different dispersion models in simulating flow at open channel bends are presented and compared. Two-dimensional governing equations are numerically solved by the finite-volume method. A standard Godunov approach based on Roe's approximate Riemann solver is used. The effects of turbulence and secondary flow were both included in the model. In Model 1, a power law distribution is assumed for longitudinal velocity and an estimation of transverse velocity at the free surface is used. Model 2 relies on an estimation of secondary flow intensity using an approximate analytical solution of the associated diffusion-dispersion equation. In Model 3, a logarithmic velocity distribution proposed by Rozovskii [2] and De Vriend [22] in transverse and streamwise directions was assumed. Experimental data of Steffler [16] at a 270° bend is used for comparison with the numerical results. The results show that Model 2 and 3 are capable of predicting the velocity redistribution phenomenon due to the effect of secondary flow at the channel bend. Model 2 gives more accurate results than Model 3 and among the models studied, it is recommended for simulation of flow at channel bends. Neglecting dispersion terms has no significant effects on water surface profiles but has a remarkable influence on the velocity field. This study shows that a suitable estimation of secondary flow intensity has a great influence on the improvement of the results of depth-averaged equations in channel bends. It seems that the numerical solution of diffusion-dispersion equation of secondary flow intensity, instead of approximate analytical solution, can improve the accuracy of the scheme, but requires more computational effort.

REFERENCES

1. Zolghadr, M., Hashemi, M. R. & Zomorodian, S. M. A. (2011). Assessment of MIKE21 model in dam and dike break simulation. *Iranian Journal of Science and Technology, Transaction B, Engineering*, Vol. 35, pp. 247-262.
2. Rozovskii, I. L. (1957). *Flow of water in bends of open channels*. Academy of Sciences of Ukrainian SSR, Kiev.
3. Kikkawa, H., Ikeda, S. & Kitagawa, A. (1976). Flow and bend topography in curved open channels. *J. Hydraul. Div.*, Vol. 102, HY9, pp. 1327-1342.
4. Flokstra, C. (1977). *Generation of two-dimensional horizontal secondary current*. Report S163, Part II, Delft Hydraulics Laboratory, The Netherlands.
5. De Vriend, D. J. (1981). Steady flow in shallow channel bends. *Communications on Hydraulics*, 81-3, Delft University of Technology, The Netherlands.
6. Odgaard, A. (1986). Meander flow model, I: Development. *J. Hydraul. Eng.* Vol. 112, pp. 1117-1136.
7. Begnudelli, L., Valiani, A. & Sandres, B.F. (2010). A Balanced Treatment of Secondary Currents, Turbulence and Dispersion in Depth-Integrated Hydrodynamic and Bed Deformation Model for Channel Bends. *Adv. Water Res.*, Vol. 33, pp. 17-33.
8. Jin, Y.C. & Steffler, P.M. (1993). Predicting flow in curved open channels by depth-averaged method. *J. Hydraul. Eng.*, Vol. 119, pp. 109-124.
9. Baek, K. O., Seo, I. W. & Lee, K. W. (2006). New equation on streamwise variation of secondary flow in meandering channels. *KSCE J. Civil Eng.* Vol.26, pp. 371-378.
10. Zeng, J., Constantinescu, G., Blanckaert, K. & Weber, L. (2008). Flow and bathymetry in sharp open-channel bends: Experiment and Predictions. *Water Resources Research*, Vol. 44, pp. 1-22.
11. Seo, I. W. & Jung, Y. J. (2010). Velocity distribution of secondary currents in curved channels. *J. Hydrodynamics*, Vol. 22, pp. 617-622.
12. Ottewanger, W., Blanckaert, K. & Uijttewaal, W. S. J. (2011). Process governing the flow redistribution in sharp river bends. *Geomorphology*, doi:10.1016/j.geomorph.2011.04.049.

13. Motta, D., Abad, J. D., Langendoen, E. J. & Garcia, M. H. (2011). A Simplified 2D Model for Meander Migration with Physically-Based Bank Evolution. *Geomorphology*, doi:10.1016/j.geomorph.2011.06.036.
14. Ghamry, H. & Steffler, P.M. (2005). Two-dimensional depth-averaged modeling of flow in curved open channels. *J. Hydraul. Res.*, Vol. 43, pp. 44-55.
15. Shimizu, Y., Yamaguchi, H. & Itakura, T. (1990). Three dimensional computation of flow and bed deformation. *J. Hydraul. Eng., ASCE*. Vol. 116, pp. 1090-1108.
16. Steffler, P. M. (1984). Turbulent flow in curved rectangular channel. PhD Thesis, University of Alberta, Edmonton, Alberta, Canada.
17. Thompson, J. F., Warsi, Z. U. A. & Mastin, C. W. (1985). *Numerical Grid Generation: Foundations and Applications*, Elsevier Science Publishing Co. Inc.
18. Baghlani, A., Talebbeydokhti, N. & Abedini, M. J. (2008). A Shock-Capturing Model Based on Flux-Vector Splitting Method in Boundary-Fitted Curvilinear Coordinates. *Applied Mathematical Modelling*. Vol. 32, pp. 249-266.
19. Kim, C. W., Yoon, T. H., Chao, Y. S. & Kim S. T. (2003). A Two-Dimensional Conservative Finite Difference Model in Nonorthogonal Coordinate System. *J. Hydraul. Res.* Vol. 41, pp. 395-403.
20. WU, W. (2007). *Computational River Dynamics*, Taylor and Francis.
21. WU, W. & WANG, S. S. Y. (2004). Depth-averaged 2-D calculation of Flow and sediment transport in curved channels. *Int. Sediment. Res.*, Vol. 19, pp. 241-257.
22. De Vriend, H.J. (1977). A Mathematical Model of Steady Flow in Curved Shallow Channels. *J. Hydraul. Res.*, Vol. 15, pp. 37-54.
23. Ahmadi, M. M, Ayyoubzadeh, S. A., Montazeri Namin, M. & Samani, J. M. V. (2009). A 2D Numerical depth-averaged model for unsteady flow in open channel bends. *J. Agr. Sci. Tech.* Vol. 11, pp. 457-468.
24. Struiksma, N., Olsen, K. W., Flokstra, C. & De Vriend, H. J. (1985). Bed deformation in curved alluvial channels. *J. Hydraul. Res.*, Vol. 23, pp. 57-79.
25. Godunov, S. K. (1959). A difference method for numerical computation of discontinuous solution of hydrodynamic equations. *Math. Sbornik*, Vol. 47, pp. 271- 306.
26. Toro, E. F. (1997). *Riemann solvers and numerical methods for fluid dynamics - A practical introduction*. Springer, New York.
27. Fujihara, M. & Borthwick, G. L. (2000). Godunov-type solution of curvilinear shallow-water equations. *J. Hydraul. Eng., ASCE*, Vol. 126, pp. 827-836.
28. Roe, P. L. (1981). Approximate Riemann Solvers, parameter vectors and difference schemes. *J. Comp. Phys.* Vol. 43, pp. 357-372.
29. Yen, B.C. (1965). Characteristics of subcritical flow in a meandering channel. *J. Hydraul. Eng. ASCE*, Vol. 119, pp. 776-795.